Available online at www.sciencedirect.com
ScienceDirect
Comput. Methods Appl. Mech. Engrg. 321 (2017) 1–17
Computer methods in applied mechanics and engineering
www.elsevier.com/locate/cma

First- and second-order energy stable methods for the modified phase field crystal equation

Hyun Geun Lee[a], Jaemin Shin[b], June-Yub Lee[c,*]

[a] Department of Mathematics, Kwangwoon University, Seoul 01897, Republic of Korea
[b] Institute of Mathematical Sciences, Ewha Womans University, Seoul 03760, Republic of Korea
[c] Department of Mathematics, Ewha Womans University, Seoul 03760, Republic of Korea

Received 22 December 2016; received in revised form 24 March 2017; accepted 25 March 2017
Available online 12 April 2017

Highlights

- We present temporally first- and second-order accurate methods for the MPFC equation.
- The unconditional stability of the proposed methods is analytically proven.
- The proposed methods represent a good balance between accuracy and energy stability.

Abstract

The phase field crystal (PFC) model was extended to the modified phase field crystal (MPFC) model, which is a sixth-order nonlinear damped wave equation, to include not only diffusive dynamics but also elastic interactions. In this paper, we present temporally first- and second-order accurate methods for the MPFC equation, which are based on an appropriate splitting of the energy for the PFC equation. And we use the Fourier spectral method for the spatial discretization. The first- and second-order methods are shown analytically to be unconditionally stable with respect to the energy and pseudoenergy of the MPFC equation, respectively. Numerical experiments are presented demonstrating the accuracy and energy stability of the proposed methods.

Keywords: Phase field crystal equation; Modified phase field crystal equation; Energy stability; Fourier spectral method

1. Introduction

Material properties are controlled by complex microstructures exhibiting topological defects, such as vacancies, grain oundaries, and dislocations. One of models for simulating these defects is the phase field crystal (PFC) equation proposed by Elder et al. [1,2]. The PFC equation is derived from a free energy functional of Swift–Hohenberg type [3]

$$\mathcal{E}(\phi) := \int_{\Omega} \left(\frac{1}{4}\phi^4 + \frac{1}{2}\phi \left(-\epsilon + (1+\Delta)^2 \right) \phi \right) d\mathbf{x}, \tag{1}$$

* Corresponding author.
E-mail address: jyllee@ewha.ac.kr (J. Lee).

http://dx.doi.org/10.1016/j.cma.2017.03.033
0045-7825/

where Ω is a domain in $\mathbb{R}^d$ ($d = 1, 2, 3$), ϕ is the atomic density field, and ϵ is a positive constant with physical significance. Under the constraint of mass conservation, the PFC equation is given by

$$\frac{\partial \phi}{\partial t} = M \Delta \mu, \tag{2}$$

where $M > 0$ is a mobility, μ is the chemical potential defined as

$$\mu := \frac{\delta \mathcal{E}}{\delta \phi} = \phi^3 - \epsilon \phi + (1 + \Delta)^2 \phi, \tag{3}$$

and $\frac{\delta \mathcal{E}}{\delta \phi}$ denotes the variational derivative of $\mathcal{E}$ with respect to ϕ. We assume that ϕ and μ are periodic on Ω. Because (2) is of gradient type, it is easy to see that the energy functional (1) is nonincreasing in time [4]. This model describes the microstructure of two-phase systems on atomic length scales but on diffusive time scales, leading to significant computational savings compared to molecular dynamics simulations which are limited by atomic length scales and femtosecond time scales. The PFC equation has been used to study various phenomena, including grain growth, dendritic and eutectic solidification, and epitaxial growth [2,5].

The PFC model evolves ϕ only on diffusive time scales [2,6], thus, it does not contain a mechanism for simulating elastic interactions, for example, the deformation properties of nanocrystalline solids. In order to overcome this problem, Stefanovic et al. [6,7] introduced the modified phase field crystal (MPFC) model that includes both diffusive dynamics and elastic interactions. The MPFC equation with periodicity is a nonlinear damped wave equation

$$\frac{\partial^2 \phi}{\partial t^2} + \beta \frac{\partial \phi}{\partial t} = M \Delta \mu, \tag{4}$$

where $\beta > 0$. Note that Eq. (4) is not a mass conservative equation due to the term $\frac{\partial^2 \phi}{\partial t^2}$. The mass conservation is an important feature required for not only the PFC equation but also the MPFC equation. Integrating Eq. (4) over Ω with the periodic boundary condition for μ and letting $\Phi(t) = \int_\Omega \frac{\partial \phi}{\partial t}\, d\mathbf{x}$, we obtain $\frac{d\Phi(t)}{dt} + \beta \Phi(t) = M \int_{\partial\Omega} \nabla \mu \cdot \mathbf{n}\, ds - M \int_\Omega \nabla \mu \cdot \nabla \mathbf{1}\, d\mathbf{x} = 0$, where $\mathbf{n}$ is a unit normal vector to $\partial\Omega$. A solution of this equation is $\Phi(t) = \Phi(0) e^{-\beta t}$. Thus, if we use an initial condition satisfying $\Phi(0) = 0$,

$$\int_\Omega \frac{\partial \phi}{\partial t}(\mathbf{x}, 0)\, d\mathbf{x} = 0, \tag{5}$$

then $\int_\Omega \frac{\partial \phi}{\partial t}(\mathbf{x}, t)\, d\mathbf{x} = 0$ for all time. We also note that the energy (1) is not necessarily nonincreasing in time along the solution trajectories of (4). However, solutions of (4) do dissipate the following energy [8]:

$$\mathcal{F}(\phi) := \mathcal{E}(\phi) + \frac{1}{2M} \left\| \frac{\partial \phi}{\partial t} \right\|_{H^{-1}}^2, \tag{6}$$

where the H^{-1} inner product is defined as follows: for given $f, g \in H_0$ (H_0 is a zero average subspace of a Hilbert space), $(f, g)_{H^{-1}} := (\nabla v_f, \nabla v_g)_{L^2}$, where $v_f, v_g \in H_0$ are the solutions of the periodic boundary value problems $-\Delta v_f = f$, $-\Delta v_g = g$ in Ω, respectively. Then, a simple calculation shows that

$$\frac{d\mathcal{F}}{dt} = \left(\mu, \frac{\partial \phi}{\partial t} \right)_{L^2} + \frac{1}{M} \left(\frac{\partial \phi}{\partial t}, \frac{\partial^2 \phi}{\partial t^2} \right)_{H^{-1}} = -\frac{\beta}{M} \left(\frac{\partial \phi}{\partial t}, \frac{\partial \phi}{\partial t} \right)_{H^{-1}} \leq 0, \tag{7}$$

where we have used the following identity [9]:

$$-\left(\Delta \mu, \frac{\partial \phi}{\partial t} \right)_{H^{-1}} = \left(\mu, \frac{\partial \phi}{\partial t} \right)_{L^2}. \tag{8}$$

This guarantees that the energy $\mathcal{F}(\phi)$ defined in (6) is nonincreasing in time.

The MPFC equation is a sixth-order nonlinear partial differential equation and cannot generally be solved analytically. Therefore, accurate and efficient numerical methods are desirable. Because of the close relationship between the PFC and MPFC models, methods for the former equation can be adapted and applied to the latter. Dehghan and Mohammadi [10] used a semi-implicit method for the PFC and MPFC equations, which splits the linear terms into backward and forward pieces while treating the nonlinear term ϕ^3 explicitly. Gomez and Nogueira [4] proposed a second-order energy stable method for the PFC equation and the method was extended to the MPFC

equation by Galenko et al. [11]. In [12–15], first- and second-order energy stable methods for the PFC equation are presented, which are based on the observation that the energy (1) can be split into two convex energies:

$$\begin{aligned}\mathcal{E}(\phi) &= \mathcal{E}^c_{\mathrm{DF}}(\phi) - \mathcal{E}^e_{\mathrm{DF}}(\phi),\\ &= \int_\Omega \left(\frac{1}{4}\phi^4 + \frac{1-\epsilon}{2}\phi^2 + \frac{1}{2}(\Delta\phi)^2\right) d\mathbf{x} - \int_\Omega |\nabla\phi|^2\, d\mathbf{x}\end{aligned} \tag{9}$$

with $\epsilon \leq 1$. Here, the diffusion (DF) term is used for $\mathcal{E}^e_{\mathrm{DF}}(\phi)$. And, in the methods, $\mathcal{E}^c_{\mathrm{DF}}(\phi)$ and $\mathcal{E}^e_{\mathrm{DF}}(\phi)$ are treated implicitly and explicitly, respectively, by following the idea in [16]. Wang and Wise [8] presented a first-order energy stable method for the MPFC equation by applying the convex splitting (9) for the PFC equation. Subsequently, a second-order energy stable method was presented in [17].

In this paper, we propose temporally first- and second-order accurate methods for the MPFC equation, which are based on the following convex splitting of the energy (1) for the PFC equation [9]:

$$\mathcal{E}^c_{\mathrm{BF}}(\phi) = \int_\Omega \left(\frac{1}{4}\phi^4 + \frac{1}{2}\phi(1+\Delta)^2\phi\right) d\mathbf{x}, \quad \mathcal{E}^e_{\mathrm{BF}}(\phi) = \int_\Omega \frac{\epsilon}{2}\phi^2\, d\mathbf{x}. \tag{10}$$

Here, the bifurcation (BF) term is used for $\mathcal{E}^e_{\mathrm{BF}}(\phi)$. The first- and second-order methods are analytically shown to be unconditionally stable with respect to the energy and pseudoenergy of the MPFC equation, respectively. We also numerically compare the proposed convex splitting methods with the previous ones based on the DF convex splitting (9).

This paper is organized as follows. In Sections 2 and 3, we propose first- and second-order energy stable methods for the MPFC equation, respectively. In Section 4, we describe numerical implementations of the proposed methods and present numerical examples showing the accuracy and energy stability of the proposed methods. Finally, conclusions are given in Section 5.

2. First-order energy stable method, $\mathrm{CS}_{\mathrm{BF}}(1)$

In this section, we present a first-order convex splitting method for the MPFC equation (4). And we will show that the method is unconditionally energy stable. Introducing a new variable ψ, one can split Eq. (4) as

$$\frac{\partial\psi}{\partial t} = M\Delta\mu - \beta\psi, \tag{11}$$

$$\frac{\partial\phi}{\partial t} = \psi \tag{12}$$

and redefine the energy (6) as

$$\mathcal{F}(\phi,\psi) := \mathcal{E}(\phi) + \frac{1}{2M}\|\psi\|^2_{H^{-1}}. \tag{13}$$

Eqs. (11) and (12) can be discretized with first-order time accuracy as follows:

$$\frac{\psi^{n+1}-\psi^n}{\Delta t} = M\Delta\mu^{n+1} - \beta\psi^{n+1}, \tag{14}$$

$$\frac{\phi^{n+1}-\phi^n}{\Delta t} = \psi^{n+1}. \tag{15}$$

In Eq. (14), μ^{n+1} can be discretized in various forms. In developing an energy stable method for the MPFC equation from the convex splitting perspective, it is important to split the energy $\mathcal{E}(\phi)$ into two convex energies appropriately and then the discretization of μ^{n+1} is determined by the splitting. Thus, an energy stability of a numerical method for the MPFC equation depends mainly on the discretization of μ^{n+1}. In [8], Wang and Wise discretized μ^{n+1} based on the splitting (9):

$$\mu^{n+1}_{\mathrm{DF}} = \frac{\delta\mathcal{E}^c_{\mathrm{DF}}}{\delta\phi}(\phi^{n+1}) - \frac{\delta\mathcal{E}^e_{\mathrm{DF}}}{\delta\phi}(\phi^n) = (\phi^{n+1})^3 + (1-\epsilon)\phi^{n+1} + \Delta^2\phi^{n+1} + 2\Delta\phi^n \tag{16}$$

and showed the method (14)–(16), referred to as $\mathrm{CS}_{\mathrm{DF}}(1)$, is unconditionally stable with respect to the energy $\mathcal{F}(\phi,\psi)$ defined in (13).

We here introduce the following discretization of μ^{n+1} based on the splitting (10):

$$\mu_{\mathrm{BF}}^{n+1} = \frac{\delta \mathcal{E}_{\mathrm{BF}}^{c}}{\delta \phi}(\phi^{n+1}) - \frac{\delta \mathcal{E}_{\mathrm{BF}}^{e}}{\delta \phi}(\phi^{n}) = (\phi^{n+1})^3 + (1+\Delta)^2\phi^{n+1} - \epsilon\phi^{n}. \tag{17}$$

Lemma 1. *The first-order convex splitting method (14), (15), and (17), referred to as CS$_{BF}$(1), for the periodic MPFC equation (4) with zero mean condition (5) is mass conserving.*

Proof. Suppose that the method $\mathrm{CS}_{\mathrm{BF}}(1)$ has a solution. From Eq. (14), we have

$$\begin{aligned}(\psi^{n+1} - \psi^{n}, \mathbf{1})_{L^2} &= M\Delta t(\Delta\mu_{\mathrm{BF}}^{n+1}, \mathbf{1})_{L^2} - \beta\Delta t(\psi^{n+1}, \mathbf{1})_{L^2} \\ &= -\beta\Delta t(\psi^{n+1}, \mathbf{1})_{L^2},\end{aligned}$$

where $(\Delta\mu_{\mathrm{BF}}^{n+1}, \mathbf{1})_{L^2} = \int_{\partial\Omega} \nabla\mu_{\mathrm{BF}}^{n+1} \cdot \mathbf{n}\, ds - \int_{\Omega} \nabla\mu_{\mathrm{BF}}^{n+1} \cdot \nabla\mathbf{1}\, d\mathbf{x} = 0$ is given by the periodic boundary condition for μ_{BF}^{n+1}. This gives the relation

$$(\psi^{n+1}, \mathbf{1})_{L^2} = \frac{1}{1+\beta\Delta t}(\psi^{n}, \mathbf{1})_{L^2}.$$

With an initial condition (5) satisfying $(\psi^0, \mathbf{1})_{L^2} = 0$, the relation ensures that $(\psi^{n+1}, \mathbf{1})_{L^2} = 0$ for all $n \geq 0$. Now, from Eq. (15), we observe that

$$(\phi^{n+1} - \phi^{n}, \mathbf{1})_{L^2} = 0 \quad \text{if and only if} \quad (\psi^{n+1}, \mathbf{1})_{L^2} = 0,$$

and the result follows: $(\phi^{n+1}, \mathbf{1})_{L^2} = (\phi^{n}, \mathbf{1})_{L^2}$. □

Theorem 2. *The method CS$_{BF}$(1) for the periodic MPFC equation (4) with zero mean condition (5) is unconditionally stable with respect to the energy $\mathcal{F}(\phi, \psi)$ defined in (13), meaning that for any time step $\Delta t > 0$,*

$$\mathcal{F}(\phi^{n+1}, \psi^{n+1}) \leq \mathcal{F}(\phi^{n}, \psi^{n}).$$

Proof. The convexity of $\mathcal{E}_{\mathrm{BF}}^{c}(\phi)$, $\mathcal{E}_{\mathrm{BF}}^{e}(\phi)$, and $\frac{1}{2M}\|\psi\|_{H^{-1}}^2$ yields the following inequalities [8]:

$$\mathcal{E}(\phi^{n+1}) - \mathcal{E}(\phi^{n}) \leq \left(\frac{\delta \mathcal{E}_{\mathrm{BF}}^{c}}{\delta \phi}(\phi^{n+1}) - \frac{\delta \mathcal{E}_{\mathrm{BF}}^{e}}{\delta \phi}(\phi^{n}), \phi^{n+1} - \phi^{n}\right)_{L^2}$$

and

$$\frac{1}{2M}\left\|\psi^{n+1}\right\|_{H^{-1}}^2 - \frac{1}{2M}\left\|\psi^{n}\right\|_{H^{-1}}^2 \leq \frac{1}{M}(\psi^{n+1}, \psi^{n+1} - \psi^{n})_{H^{-1}}.$$

Using these inequalities, we have

$$\begin{aligned}\mathcal{F}(\phi^{n+1}, \psi^{n+1}) - \mathcal{F}(\phi^{n}, \psi^{n}) &\leq (\mu_{\mathrm{BF}}^{n+1}, \Delta t\psi^{n+1})_{L^2} + \frac{1}{M}(\psi^{n+1}, \psi^{n+1} - \psi^{n})_{H^{-1}} \\ &= \left(\psi^{n+1}, -\Delta t\Delta\mu_{\mathrm{BF}}^{n+1} + \frac{1}{M}(\psi^{n+1} - \psi^{n})\right)_{H^{-1}} \\ &= -\frac{\beta\Delta t}{M}(\psi^{n+1}, \psi^{n+1})_{H^{-1}} \leq 0,\end{aligned}$$

where $(\mu_{\mathrm{BF}}^{n+1}, \Delta t\psi^{n+1})_{L^2} = (\psi^{n+1}, -\Delta t\Delta\mu_{\mathrm{BF}}^{n+1})_{H^{-1}}$ is given by the identity (8). □

3. Second-order energy stable method, CS$_{\mathrm{BF}}$(2)

In this section, we present a second-order convex splitting method for the MPFC equation, which can be described in a similar way to $\mathrm{CS}_{\mathrm{BF}}(1)$. Eqs. (11) and (12) can be discretized with second-order time accuracy as follows:

$$\frac{\psi^{n+1} - \psi^{n}}{\Delta t} = M\Delta\mu^{n+\frac{1}{2}} - \beta\frac{\psi^{n+1} + \psi^{n}}{2}, \tag{18}$$

$$\frac{\phi^{n+1} - \phi^{n}}{\Delta t} = \frac{\psi^{n+1} + \psi^{n}}{2}. \tag{19}$$

In [17], Baskaran et al. discretized $\mu^{n+\frac{1}{2}}$ based on the splitting (9):

$$\mu_{\mathrm{DF}}^{n+\frac{1}{2}} = \frac{(\phi^{n+1})^2+(\phi^n)^2}{2}\frac{\phi^{n+1}+\phi^n}{2} + (1-\epsilon)\frac{\phi^{n+1}+\phi^n}{2} + \Delta^2\left(\frac{\phi^{n+1}+\phi^n}{2}\right) + \Delta(3\phi^n-\phi^{n-1}), \tag{20}$$

where $\phi^{-1} = \phi^0$. Here, $\frac{\delta\mathcal{E}_{\mathrm{DF}}^c}{\delta\phi}$ is treated implicitly using a second-order secant type approach and $\frac{\delta\mathcal{E}_{\mathrm{DF}}^e}{\delta\phi}$ is treated explicitly using a second-order extrapolation. The authors showed the method (18)–(20), referred to as $\mathrm{CS}_{\mathrm{DF}}(2)$, is unconditionally stable with respect to the following pseudoenergy:

$$\mathcal{F}_{\mathrm{DF}}(\phi^n,\phi^{n-1},\psi^n) := \mathcal{F}(\phi^n,\psi^n) + \frac{1}{2}\|\nabla(\phi^n-\phi^{n-1})\|_{L^2}^2. \tag{21}$$

In other words, for any $\Delta t > 0$,

$$\mathcal{F}_{\mathrm{DF}}(\phi^{n+1},\phi^n,\psi^{n+1}) \le \mathcal{F}_{\mathrm{DF}}(\phi^n,\phi^{n-1},\psi^n).$$

We here introduce the following discretization of $\mu^{n+\frac{1}{2}}$ based on the splitting (10):

$$\mu_{\mathrm{BF}}^{n+\frac{1}{2}} = \frac{(\phi^{n+1})^2+(\phi^n)^2}{2}\frac{\phi^{n+1}+\phi^n}{2} + (1+\Delta)^2\left(\frac{\phi^{n+1}+\phi^n}{2}\right) - \epsilon\frac{3\phi^n-\phi^{n-1}}{2}. \tag{22}$$

Lemma 3. *The second-order convex splitting method (18), (19), and (22), referred to as $CS_{BF}(2)$, for the periodic MPFC equation (4) with zero mean condition (5) is mass conserving.*

Proof. The proof for the method $\mathrm{CS}_{\mathrm{BF}}(2)$ is similar to the proof for the method $\mathrm{CS}_{\mathrm{BF}}(1)$ in Lemma 1. □

Theorem 4. *The method $CS_{BF}(2)$ for the periodic MPFC equation (4) with zero mean condition (5) is unconditionally stable with respect to the following pseudoenergy:*

$$\mathcal{F}_{BF}(\phi^n,\phi^{n-1},\psi^n) := \mathcal{F}(\phi^n,\psi^n) + \frac{\epsilon}{4}\|\phi^n-\phi^{n-1}\|_{L^2}^2. \tag{23}$$

In other words, for any $\Delta t > 0$,

$$\mathcal{F}_{BF}(\phi^{n+1},\phi^n,\psi^{n+1}) \le \mathcal{F}_{BF}(\phi^n,\phi^{n-1},\psi^n).$$

Proof. Let $\psi^{n+\frac{1}{2}} = \frac{\psi^{n+1}+\psi^n}{2}$ for simplicity of notation. Using the identities

$$\left(\phi^{n+1}-\phi^n, -\epsilon\frac{3\phi^n-\phi^{n-1}}{2}\right)_{L^2} + \frac{\epsilon}{2}\|\phi^{n+1}\|_{L^2}^2 - \frac{\epsilon}{2}\|\phi^n\|_{L^2}^2$$
$$= \frac{\epsilon}{4}\|\phi^{n+1}-\phi^n\|_{L^2}^2 - \frac{\epsilon}{4}\|\phi^n-\phi^{n-1}\|_{L^2}^2 + \frac{\epsilon}{4}\|\phi^{n+1}-2\phi^n+\phi^{n-1}\|_{L^2}^2$$

and

$$\left(\phi^{n+1}-\phi^n, \frac{(\phi^{n+1})^2+(\phi^n)^2}{2}\frac{\phi^{n+1}+\phi^n}{2} + (1+\Delta)^2\left(\frac{\phi^{n+1}+\phi^n}{2}\right)\right)_{L^2}$$
$$= \mathcal{E}(\phi^{n+1}) - \mathcal{E}(\phi^n) + \frac{\epsilon}{2}\|\phi^{n+1}\|_{L^2}^2 - \frac{\epsilon}{2}\|\phi^n\|_{L^2}^2,$$

we obtain

$$\begin{aligned}(\Delta t\,\psi^{n+\frac{1}{2}}, \mu_{\mathrm{BF}}^{n+\frac{1}{2}})_{L^2} &= (\phi^{n+1}-\phi^n, \mu_{\mathrm{BF}}^{n+\frac{1}{2}})_{L^2}\\ &= \mathcal{E}(\phi^{n+1}) + \frac{\epsilon}{4}\|\phi^{n+1}-\phi^n\|_{L^2}^2 - \mathcal{E}(\phi^n) - \frac{\epsilon}{4}\|\phi^n-\phi^{n-1}\|_{L^2}^2\\ &\quad + \frac{\epsilon}{4}\|\phi^{n+1}-2\phi^n+\phi^{n-1}\|_{L^2}^2.\end{aligned} \tag{24}$$

Next, from Eq. (18), we have

$$\begin{aligned} -(\psi^{n+\frac{1}{2}}, \Delta t \mu_{\mathrm{BF}}^{n+\frac{1}{2}})_{L^2} &= \frac{1}{M}(\psi^{n+\frac{1}{2}}, M\Delta t \Delta \mu_{\mathrm{BF}}^{n+\frac{1}{2}})_{H^{-1}} \\ &= \frac{1}{M}(\psi^{n+\frac{1}{2}}, \psi^{n+1} - \psi^n + \beta \Delta t \psi^{n+\frac{1}{2}})_{H^{-1}} \\ &= \frac{1}{2M}\|\psi^{n+1}\|_{H^{-1}}^2 - \frac{1}{2M}\|\psi^n\|_{H^{-1}}^2 + \frac{\beta \Delta t}{M}\|\psi^{n+\frac{1}{2}}\|_{H^{-1}}^2. \end{aligned} \tag{25}$$

Adding Eqs. (24) and (25), we obtain

$$\begin{aligned} &\mathcal{F}_{\mathrm{BF}}(\phi^{n+1}, \phi^n, \psi^{n+1}) - \mathcal{F}_{\mathrm{BF}}(\phi^n, \phi^{n-1}, \psi^n) \\ &\quad = -\frac{\beta \Delta t}{M}\|\psi^{n+\frac{1}{2}}\|_{H^{-1}}^2 - \frac{\epsilon}{4}\|\phi^{n+1} - 2\phi^n + \phi^{n-1}\|_{L^2}^2 \le 0. \quad \square \end{aligned}$$

4. Numerical experiments

4.1. Numerical implementations of $CS_{BF}(1)$ and $CS_{BF}(2)$

The method $\mathrm{CS}_{\mathrm{BF}}(1)$ defined in Section 2 can be simplified as follows:

$$\frac{\phi^{n+1} - \phi^n}{\Delta t} = \frac{M\Delta t}{1 + \beta \Delta t}\Delta\left((\phi^{n+1})^3 + (1+\Delta)^2\phi^{n+1} - \epsilon\phi^n\right) + \frac{1}{1+\beta\Delta t}\psi^n, \tag{26}$$

$$\psi^{n+1} = \frac{\phi^{n+1} - \phi^n}{\Delta t}. \tag{27}$$

We solve ϕ^{n+1} using Eq. (26) and then update ψ^{n+1} by Eq. (27) for the next time level. The nonlinearity in Eq. (26) comes from the cubic term $(\phi^{n+1})^3$ and this can be handled using a Newton-type linearization [9,13,17]

$$(\phi^{n,m+1})^3 \approx (\phi^{n,m})^3 + 3(\phi^{n,m})^2(\phi^{n,m+1} - \phi^{n,m})$$

for $m = 0, 1, \ldots$. We then develop a Newton-type fixed point iteration method as

$$\begin{aligned} &\left[I - \frac{M\Delta t^2}{1+\beta\Delta t}\Delta\left(3(\phi^{n,m})^2 + (1+\Delta)^2\right)\right]\phi^{n,m+1} \\ &\quad = \phi^n + \frac{M\Delta t^2}{1+\beta\Delta t}\Delta\left(-2(\phi^{n,m})^3 - \epsilon\phi^n\right) + \frac{\Delta t}{1+\beta\Delta t}\psi^n, \end{aligned} \tag{28}$$

where $\phi^{n,0} = \phi^n$, and we set

$$\phi^{n+1} = \phi^{n,m+1}$$

if a relative l_2-norm of the consecutive error $\frac{\|\phi^{n,m+1} - \phi^{n,m}\|_2}{\|\phi^{n,m}\|_2}$ is less than a tolerance tol (is set to $10^{-8}\Delta t$ in this paper).

In this paper, the biconjugate gradient (BICG) method is used to solve the system (28) and we use the following preconditioner P to accelerate the convergence speed of the BICG algorithm:

$$P = I - \frac{M\Delta t^2}{1+\beta\Delta t}\Delta\left(\bar{A}I + (1+\Delta)^2\right),$$

where $\bar{A}$ is the average value of $3(\phi^{n,m})^2$. The stopping criterion for the BICG iteration is that the relative residual norm is less than tol (is set to $10^{-8}\Delta t$ in this paper).

And we emphasize time discretization since the energy stability in time is the central issue. In particular, our time stepping method $\mathrm{CS}_{\mathrm{BF}}$ can be combined with any spatial discretization (e.g., finite difference [8,9,17], finite element [4,11], radial basis function [18] methods) as long as the spatial discretization provides the desired tolerance. We here use the Fourier spectral method for the spatial discretization and the fast Fourier transform in MATLAB is applied for the whole numerical simulations to solve the MPFC equation with the periodic boundary condition.

The method $\mathrm{CS}_{\mathrm{BF}}(2)$ defined in Section 3 can be simplified as follows:

$$\frac{\phi^{n+1}-\phi^n}{\Delta t} = \frac{M\Delta t}{2+\beta\Delta t}\Delta\left(\frac{(\phi^{n+1})^2+(\phi^n)^2}{2}\frac{\phi^{n+1}+\phi^n}{2}+(1+\Delta)^2\left(\frac{\phi^{n+1}+\phi^n}{2}\right)\right.$$
$$\left.-\epsilon\frac{3\phi^n-\phi^{n-1}}{2}\right)+\frac{2}{2+\beta\Delta t}\psi^n, \tag{29}$$

$$\psi^{n+1} = 2\frac{\phi^{n+1}-\phi^n}{\Delta t}-\psi^n. \tag{30}$$

We solve ϕ^{n+1} using Eq. (29) and then update ψ^{n+1} by Eq. (30) for the next time level. Using the linearizations

$$(\phi^{n,m+1})^3 \approx (\phi^{n,m})^3+3(\phi^{n,m})^2(\phi^{n,m+1}-\phi^{n,m}),$$
$$(\phi^{n,m+1})^2 \approx (\phi^{n,m})^2+2\phi^{n,m}(\phi^{n,m+1}-\phi^{n,m}),$$

we develop a Newton-type fixed point iteration method as

$$\left[I-\frac{M\Delta t^2}{2+\beta\Delta t}\Delta\left(\frac{3(\phi^{n,m})^2+2\phi^{n,m}\phi^n+(\phi^n)^2}{4}+\frac{1}{2}(1+\Delta)^2\right)\right]\phi^{n,m+1}$$
$$=\phi^n+\frac{M\Delta t^2}{2+\beta\Delta t}\Delta\left(\frac{-2(\phi^{n,m})^3-(\phi^{n,m})^2\phi^n+(\phi^n)^3}{4}+\frac{1}{2}(1+\Delta)^2\phi^n\right.$$
$$\left.-\epsilon\frac{3\phi^n-\phi^{n-1}}{2}\right)+\frac{2\Delta t}{2+\beta\Delta t}\psi^n. \tag{31}$$

For the system (31), we use the following preconditioner P:

$$P = I-\frac{M\Delta t^2}{2+\beta\Delta t}\Delta\left(\bar{A}I+\frac{1}{2}(1+\Delta)^2\right),$$

where $\bar{A}$ is the average value of $\frac{3(\phi^{n,m})^2+2\phi^{n,m}\phi^n+(\phi^n)^2}{4}$. The other components of the numerical algorithm of the method $\mathrm{CS}_{\mathrm{BF}}(2)$ are the same as those of the method $\mathrm{CS}_{\mathrm{BF}}(1)$.

4.2. Numerical convergence with a smooth test function in 1D

We demonstrate the convergence of the proposed methods $\mathrm{CS}_{\mathrm{BF}}(1)$ and $\mathrm{CS}_{\mathrm{BF}}(2)$ with an initial condition

$$\phi(x,0) = 0.07-0.02\cos\left(\frac{2\pi(x-12)}{32}\right)+0.02\cos^2\left(\frac{\pi(x+10)}{32}\right)$$
$$-0.01\sin^2\left(\frac{4\pi x}{32}\right), \qquad \psi(x,0)=0 \tag{32}$$

on $\Omega=[0,32]$. We set $M=1$ and $\epsilon=0.25$, and the grid size is fixed to $\Delta x=1/2$ which provides enough spatial accuracy. In order to estimate the convergence rate with respect to Δt, simulations are performed by varying $\Delta t = 100\beta/2^{13}, 100\beta/2^{12}, \ldots, 100\beta/2^3$ for $\beta=0.1$, 1, and 10. We take the quadruply over-resolved numerical solution using the method $\mathrm{CS}_{\mathrm{BF}}(2)$ as the reference solution.

For $\beta=1$, Fig. 1 shows the evolution of the reference solution $\phi(x,t)$. The initial oscillation changes little by little until a new oscillation is generated. Then the new oscillation grows for a relatively short time and reaches a steady state.

In order to show the robustness of the nonlinear solver and the necessity of the preconditioner, we count the number of nonlinear and BICG iterations for the method $\mathrm{CS}_{\mathrm{BF}}(2)$. The number of nonlinear iterations averaged over the simulation time $0<t=n\Delta t\le 100$ is shown as a function of Δt in Fig. 2(a). The stopping criterion for the nonlinear iteration is that a relative l_2-norm of the consecutive error is less than $tol=10^{-8}\Delta t$. On average, 2–4 nonlinear iterations were involved in proceeding to the next time level. We believe that such a fast iterative convergence can be achieved since the successive iteration (31) is a Newton-type fixed point iteration method. And the number of BICG iterations averaged over the simulation time is shown as a function of Δt in Fig. 2(b). Here, we regard the number of BICG iterations at each time level as the averaged number of BICG iterations for the nonlinear iterations at each time

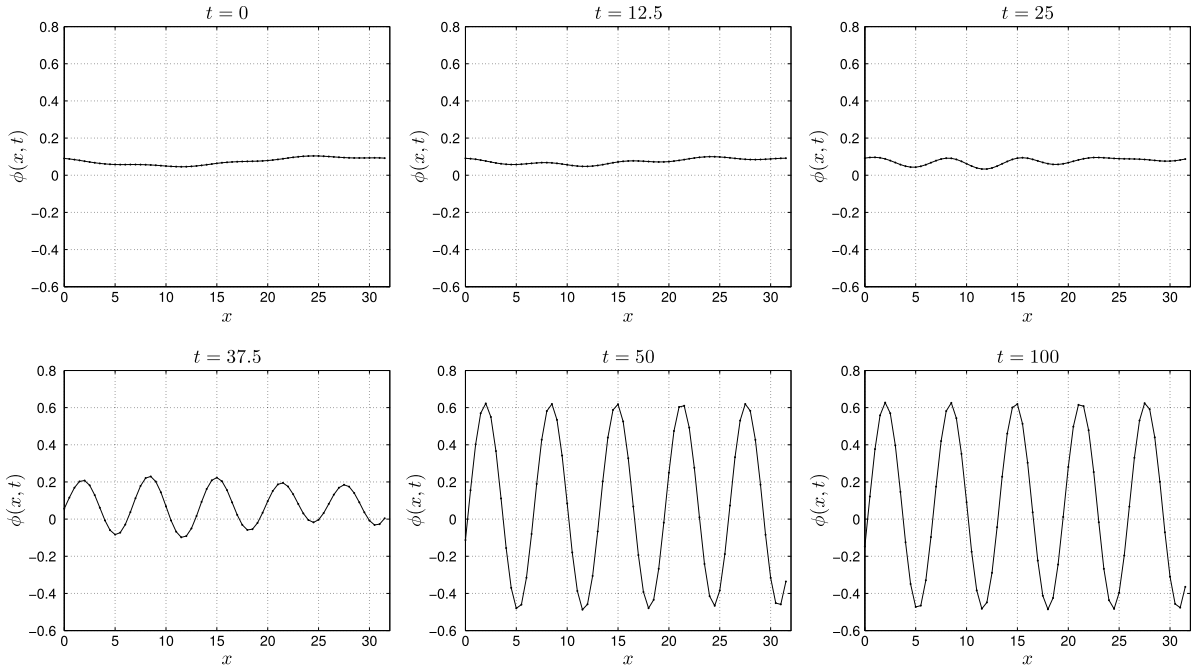

Fig. 1. Evolution of the reference solution $\phi(x, t)$ with $\beta = 1$ and $\epsilon = 0.25$.

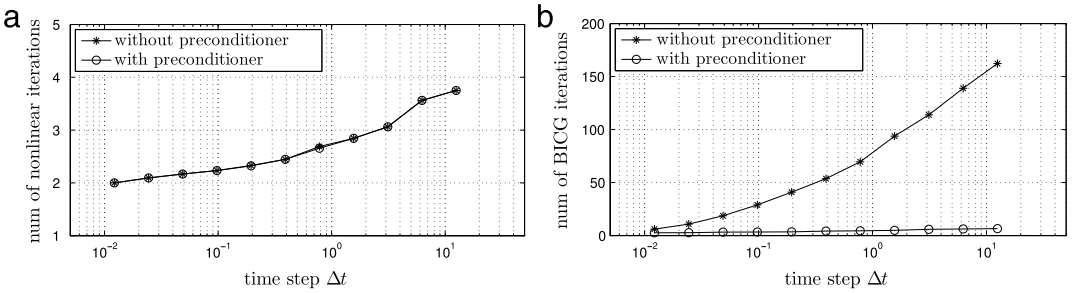

Fig. 2. Number of (a) nonlinear and (b) BICG iterations for the method $CS_{BF}(2)$.

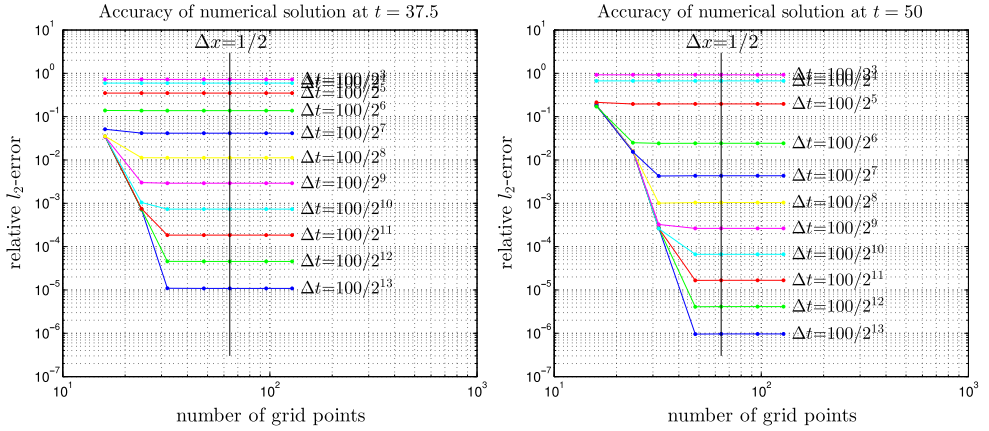

Fig. 3. Relative l_2-errors of $\phi(x, t)$ at $t = 37.5$ and 50 for $16, 24, 32, \ldots, 128$ grid points and $\Delta t = 100/2^{13}, \ldots, 100/2^3$. Here, $\beta = 1$ and $\epsilon = 0.25$, and the method $CS_{BF}(2)$ is used.

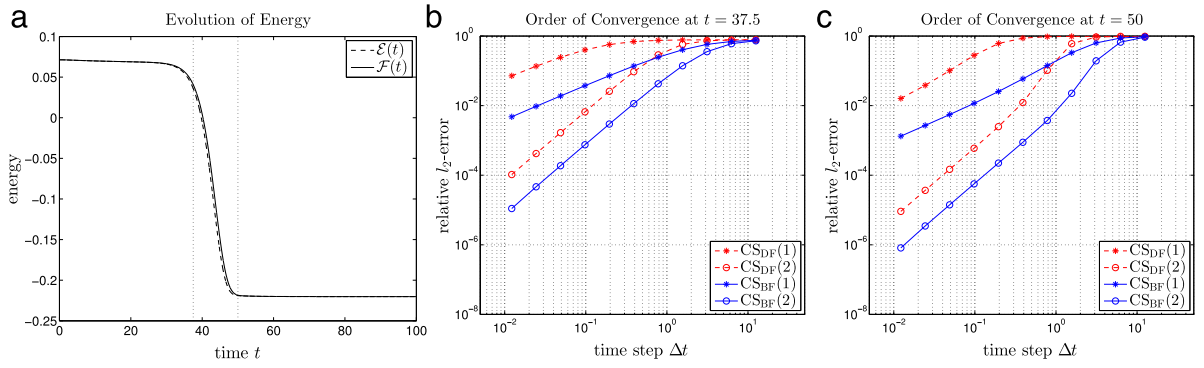

Fig. 4. (a) Evolution of the energies $\mathcal{E}(t)$ and $\mathcal{F}(t)$ with $\beta = 1$ and $\epsilon = 0.25$. (b)–(c) Relative l_2-errors of $\phi(x, t)$ at $t = 37.5$ and 50 for $\Delta t = 100/2^{13}, \ldots, 100/2^3$.

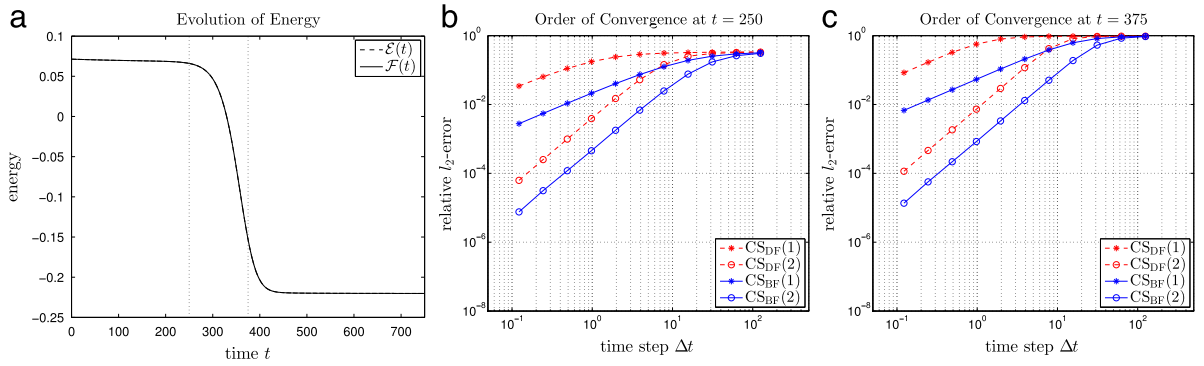

Fig. 5. (a) Evolution of the energies $\mathcal{E}(t)$ and $\mathcal{F}(t)$ with $\beta = 10$ and $\epsilon = 0.25$. (b)–(c) Relative l_2-errors of $\phi(x, t)$ at $t = 250$ and 375 for $\Delta t = 1000/2^{13}, \ldots, 1000/2^3$.

level, and the stopping criterion for the BICG iteration is that the relative residual norm is less than $tol = 10^{-8}\Delta t$. As shown in Fig. 2(b), the BICG iterations were remarkably reduced by using the preconditioner.

Next, to show spatial accuracy of the numerical solution, we take the same initial condition (32) and parameter values used to create Fig. 1. Simulations are performed by using the method $\mathrm{CS_{BF}}(2)$ and varying the number of grid points 16, 24, 32, …, 128. Fig. 3 shows the relative l_2-errors of $\phi(x, t)$ at $t = 37.5$ and 50 for various numbers of grid points and time steps. Here, the errors are computed by comparison with the reference solution using 256 grid points and $\Delta t = 100/2^{15}$. As we can see in Fig. 3, the spatial convergence of the method under grid refinement is evident and 64 grid points ($\Delta x = 1/2$) give sufficient spatial accuracy.

The evolution of the energies $\mathcal{E}(t)$ and $\mathcal{F}(t)$ for the reference solution $\phi(x, t)$ is shown in Fig. 4(a). At an early stage, both energies evolve slowly, and then decay rapidly. The flat end in Fig. 4(a) indicates that a steady state is reached. Figs. 4(b) and (c) show the relative l_2-errors of $\phi(x, t)$ at $t = 37.5$ and 50 (these times are indicated by dotted lines in Fig. 4(a)) for various time steps. Here, the errors are computed by comparison with the reference solution in Fig. 1. It is observed that both methods $\mathrm{CS_{DF}}$ and $\mathrm{CS_{BF}}$ give desired order of accuracy in time.

Figs. 5(a) and 6(a) show the evolutions of the energies for the reference solutions $\phi(x, t)$ with $\beta = 10$ and 0.1, respectively. When β is large ($\beta = 10$, high damping case), the MPFC model behaves like the PFC model and $\mathcal{F}(t)$ is nearly identical to $\mathcal{E}(t)$. On the other hand, when β is small ($\beta = 0.1$, low damping case), $\mathcal{F}(t)$ differs from $\mathcal{E}(t)$ and, in particular, $\mathcal{E}(t)$ shows an oscillatory behavior unlike the case with $\beta = 10$. For the high and low damping cases, Figs. 5 and 6(b)–(c) show the relative l_2-errors of $\phi(x, t)$ at different times (these times are indicated by dotted lines in Figs. 5 and 6(a)) for various time steps. It is also observed that both methods $\mathrm{CS_{DF}}$ and $\mathrm{CS_{BF}}$ give desired order of accuracy in time; however, the methods $\mathrm{CS_{BF}}(1)$ and $\mathrm{CS_{BF}}(2)$ for all β used in this section are one order of magnitude more accurate than the methods $\mathrm{CS_{DF}}(1)$ and $\mathrm{CS_{DF}}(2)$, respectively.

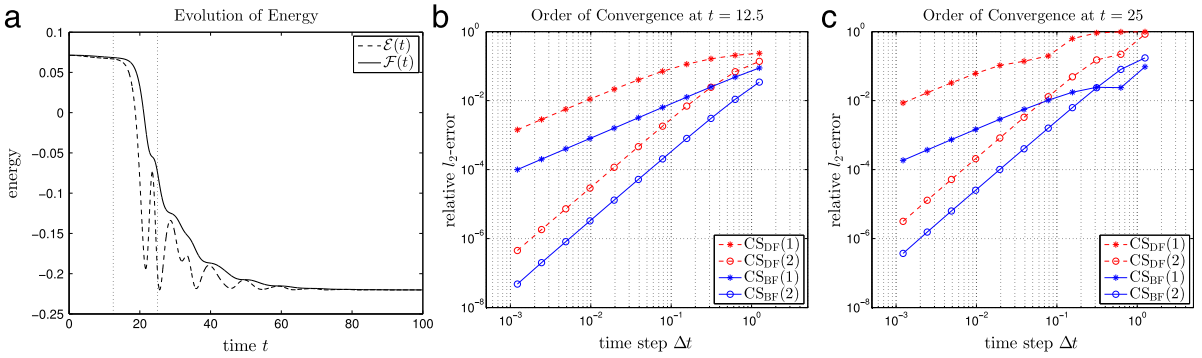

Fig. 6. (a) Evolution of the energies $\mathcal{E}(t)$ and $\mathcal{F}(t)$ with $\beta = 0.1$ and $\epsilon = 0.25$. (b)–(c) Relative l_2-errors of $\phi(x, t)$ at $t = 12.5$ and 25 for $\Delta t = 10/2^{13}, \ldots, 10/2^3$.

4.3. Numerical dissipation with a smooth test function in 1D

In order to compare methods with the same order of convergence, a concept similar to that of an error constant is needed. In [19], Guillén-González and Tierra introduced the numerical dissipation of methods as the concept for the Cahn–Hilliard equation [20,21] and concluded that a method with smaller numerical dissipation is more accurate. In order to compare the methods CS_{DF} and CS_{BF}, we define the numerical dissipation of methods for the MPFC equation as follows:

$$\mathrm{ND} := \mathrm{ND}_1 + \mathrm{ND}_2,$$

where

$$\mathrm{ND}_1 = \frac{1}{\Delta t}\left(\frac{\delta \mathcal{E}}{\delta \phi}(\phi^{n+1}, \phi^n), \phi^{n+1} - \phi^n\right)_{L^2} - \frac{1}{\Delta t}\left(\mathcal{E}(\phi^{n+1}) - \mathcal{E}(\phi^n)\right) \tag{33}$$

and

$$\mathrm{ND}_2 = \frac{1}{2M\Delta t}\left(\frac{\delta \|\psi\|^2_{H^{-1}}}{\delta \psi}(\psi^{n+1}, \psi^n), \psi^{n+1} - \psi^n\right)_{H^{-1}} - \frac{1}{2M\Delta t}\left(\|\psi^{n+1}\|^2_{H^{-1}} - \|\psi^n\|^2_{H^{-1}}\right). \tag{34}$$

Here, $\frac{\delta \mathcal{E}}{\delta \phi}(\phi^{n+1}, \phi^n)$ and $\frac{\delta \|\psi\|^2_{H^{-1}}}{\delta \psi}(\psi^{n+1}, \psi^n)$ must be defined by a numerical method. In a CS method, ND_1 is defined with

$$\frac{\delta \mathcal{E}}{\delta \phi}(\phi^{n+1}, \phi^n) = \mu^{n+p},$$

where $p = 1$ and $\frac{1}{2}$ for the first- and second-order methods, respectively. And ND_2 is defined with

$$\frac{\delta \|\psi\|^2_{H^{-1}}}{\delta \psi}(\psi^{n+1}, \psi^n) = 2\psi^{n+p},$$

where $\psi^{n+p} = p\psi^{n+1} + (1-p)\psi^n$. We remark that $\mathrm{ND}_2 = \frac{1}{2M\Delta t}\|\psi^{n+1} - \psi^n\|^2_{H^{-1}} \geq 0$ when $p = 1$ and $\mathrm{ND}_2 = 0$ when $p = \frac{1}{2}$. From (33) and (34), we have

$$\mathrm{ND} = -\frac{\mathcal{F}(\phi^{n+1}, \psi^{n+1}) - \mathcal{F}(\phi^n, \psi^n)}{\Delta t} - \frac{\beta}{M}\|\psi^{n+p}\|^2_{H^{-1}}. \tag{35}$$

For $\beta = 0.1$, we compute the numerical dissipation (35) of the methods CS_{DF} and CS_{BF} with the same initial condition (32) and parameter values used in the previous section. Figs. 7 and 8 show the evolution of the numerical dissipation of the first- and second-order methods, respectively, with $\Delta t = 10/2^9, 10/2^8$, and $10/2^7$ (these time steps lie in the convergence region of both methods CS_{DF} and CS_{BF}, see Figs. 6(b) and (c)). In Fig. 7, both methods $CS_{DF}(1)$ and $CS_{BF}(1)$ have nonnegative numerical dissipations over the whole evolution; $\mathrm{ND} \geq 0$ implies that $\mathcal{F}(\phi^{n+1}, \psi^{n+1}) \leq \mathcal{F}(\phi^n, \psi^n)$. From the results in Figs. 7 and 8, we can see that the numerical dissipations of the proposed methods, $CS_{BF}(1)$ and $CS_{BF}(2)$, are less than those of the counterparts, $CS_{DF}(1)$ and $CS_{DF}(2)$.

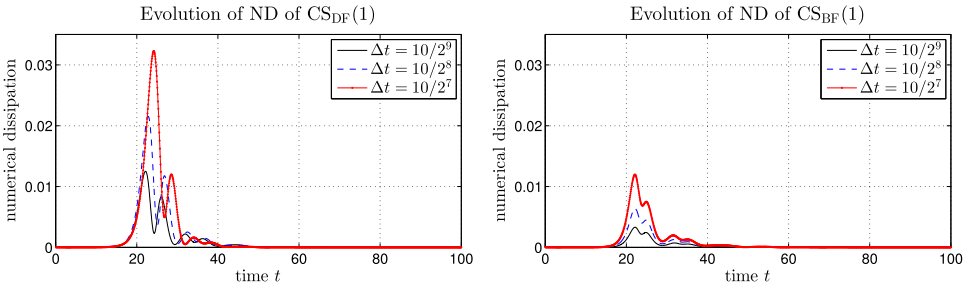

Fig. 7. Evolution of the numerical dissipation of the first-order methods with different time steps.

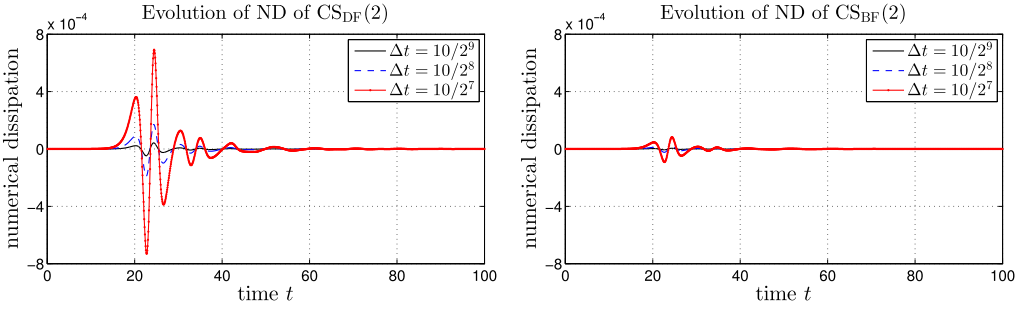

Fig. 8. Evolution of the numerical dissipation of the second-order methods with different time steps.

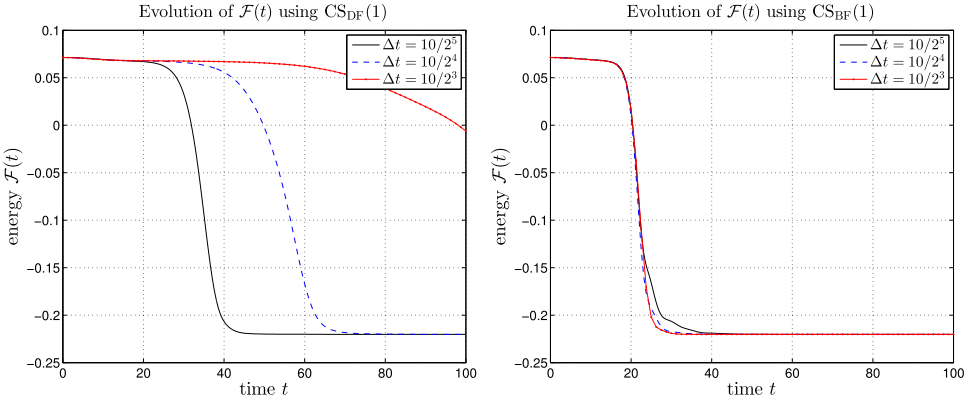

Fig. 9. Evolution of the energy $\mathcal{F}(t)$ using the first-order methods with different time steps.

4.4. Energy stability with a smooth test function in 1D

Next, we investigate the effect of time step on the energy evolution. To this, we take $\beta = 0.1$ with the same initial condition (32) and parameter values used in Section 4.2. Fig. 9 shows the evolution of the energy $\mathcal{F}(t)$ using the first-order methods with $\Delta t = 10/2^5$, $10/2^4$, and $10/2^3$ (these time steps are sufficiently large, see Figs. 6(b) and (c)). All the energy curves are nonincreasing in time, however, the energies using the method $CS_{BF}(1)$ with different time steps are almost similar, whereas significant differences emerge with large time steps for the method $CS_{DF}(1)$.

For the second-order methods, the energy that is guaranteed to be nonincreasing in time is the pseudoenergy $\mathcal{F}_{DF}(t)$ defined in (21) and $\mathcal{F}_{BF}(t)$ defined in (23). When the time step is small enough, $\mathcal{F}(t)$ is close to $\mathcal{F}_{DF}(t)$ or $\mathcal{F}_{BF}(t)$, and thus $\mathcal{F}(t)$ is nonincreasing in time (see Fig. 6(a)). However, the difference between $\mathcal{F}(t)$ and $\mathcal{F}_{DF}(t)$ or $\mathcal{F}_{BF}(t)$ becomes bigger as the time step increases, and thus $\mathcal{F}(t)$ is not guaranteed to be nonincreasing in time.

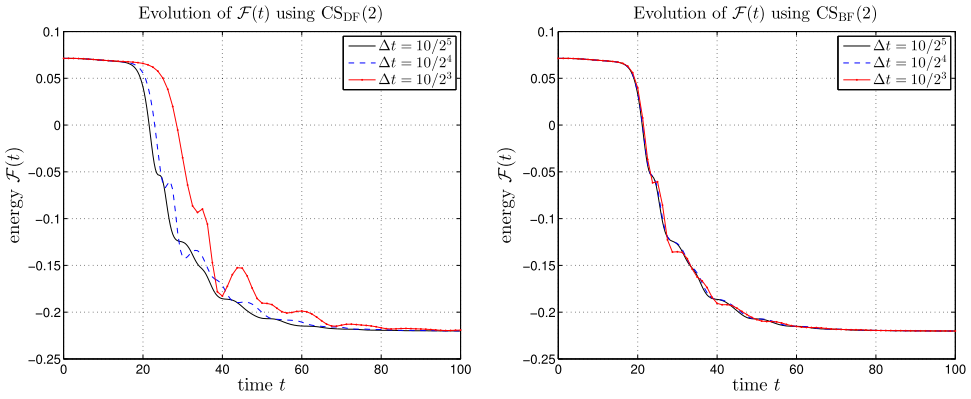

Fig. 10. Evolution of the energy $\mathcal{F}(t)$ using the second-order methods with different time steps.

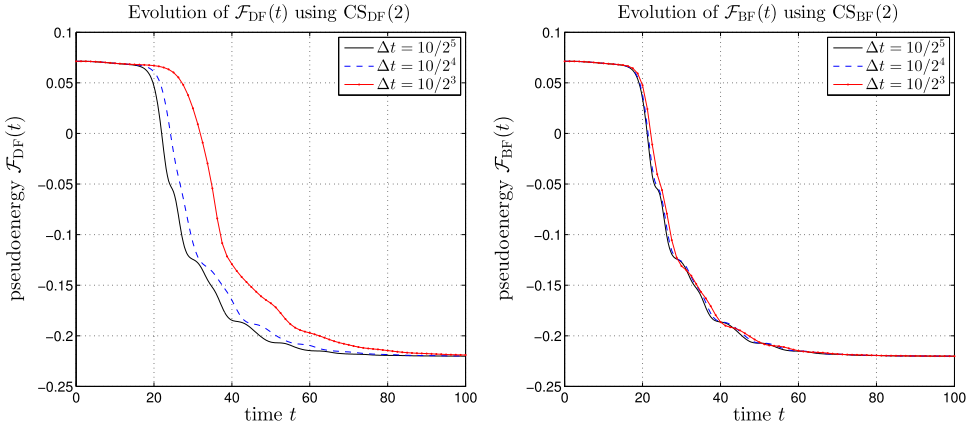

Fig. 11. Evolution of the pseudoenergies $\mathcal{F}_{\mathrm{DF}}(t)$ and $\mathcal{F}_{\mathrm{BF}}(t)$ with different time steps.

Fig. 10 shows the evolution of the energy $\mathcal{F}(t)$ using the second-order methods with different time steps. In the case of the method $\mathrm{CS}_{\mathrm{DF}}(2)$, the energy dissipation property (7) starts to break down when $\Delta t = 10/2^4$ and $\mathcal{F}(t)$ with $\Delta t = 10/2^3$ is significantly oscillating in time. However, in the case of the method $\mathrm{CS}_{\mathrm{BF}}(2)$, $\mathcal{F}(t)$ with $\Delta t = 10/2^4$ is still nonincreasing in time and $\mathcal{F}(t)$ with $\Delta t = 10/2^3$ is nearly nonincreasing in time.

Fig. 11 shows the evolution of the pseudoenergies $\mathcal{F}_{\mathrm{DF}}(t)$ and $\mathcal{F}_{\mathrm{BF}}(t)$ with different time steps. All the pseudoenergy curves are nonincreasing in time. We also observe that the time step effect on the pseudoenergy evolution is more alleviated using the method $\mathrm{CS}_{\mathrm{BF}}(2)$ than $\mathrm{CS}_{\mathrm{DF}}(2)$. From the results in Figs. 9–11, we conclude that the proposed methods represent a good balance between accuracy and energy stability.

4.5. Numerical convergence with a nonsmooth test function in 1D

In this section, we demonstrate the convergence of the proposed methods with the same parameter values used to create Fig. 6 except for initial condition and time step. We here take an initial condition as

$$\phi(x, 0) = 0.02 + \mathrm{rand}, \qquad \psi(x, 0) = 0, \tag{36}$$

where rand is a random number between -0.1 and 0.1 at the grid points. Unlike the case of the smooth initial condition (32), a much smaller time step is needed to deal with the high frequency modes in the initial condition (36). Thus, we vary $\Delta t = 2^{-19}, 2^{-18}, \ldots, 2^{-6}$ to estimate the convergence rate with respect to Δt for the random initial condition. We take the quadruply over-resolved numerical solution using the method $\mathrm{CS}_{\mathrm{BF}}(2)$ as the reference solution.

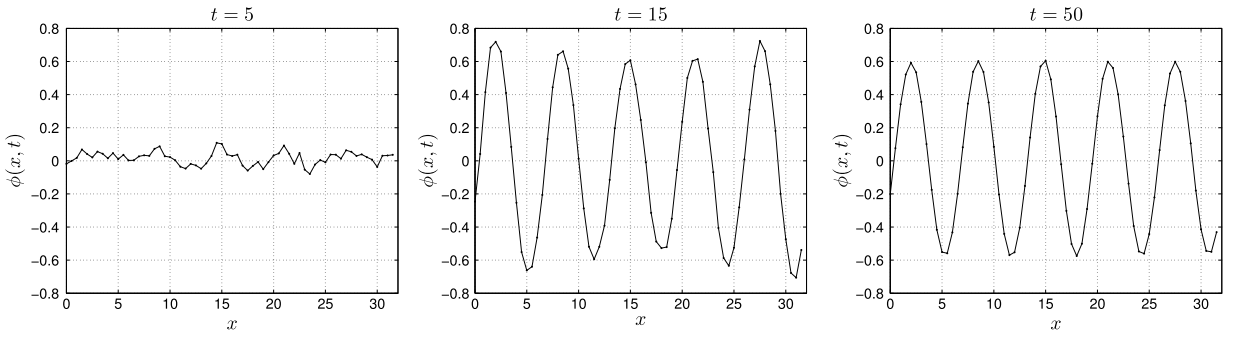

Fig. 12. Evolution of the reference solution $\phi(x, t)$ with $\beta = 0.1$ and $\epsilon = 0.25$.

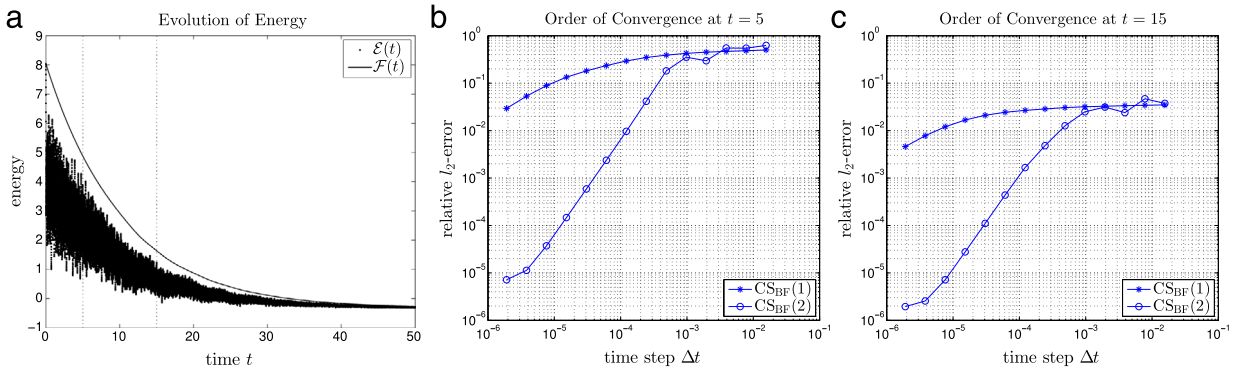

Fig. 13. (a) Evolution of the energies $\mathcal{E}(t)$ and $\mathcal{F}(t)$ with $\beta = 0.1$ and $\epsilon = 0.25$. (b)–(c) Relative l_2-errors of $\phi(x, t)$ at $t = 5$ and 15 for $\Delta t = 2^{-19}, 2^{-18}, \ldots, 2^{-6}$.

The evolution of the reference solution $\phi(x, t)$ and of the energies $\mathcal{E}(t)$ and $\mathcal{F}(t)$ is shown in Figs. 12 and 13(a), respectively. And the relative l_2-errors of $\phi(x, t)$ at $t = 5$ and 15 (these times are indicated by dotted lines in Fig. 13(a)) for various time steps are shown in Figs. 13(b) and (c). It is observed that the methods $\mathrm{CS}_{\mathrm{BF}}(1)$ and $\mathrm{CS}_{\mathrm{BF}}(2)$ give desired order of accuracy in time even for the random initial condition.

4.6. Time evolution of random perturbation in 2D

We solve the MPFC equation (4) on $\Omega = [0, 32] \times [0, 32]$ with $\beta = 0.1$, $M = 1$, $\epsilon = 0.2$, and $\Delta x = \Delta y = 0.5$. An initial condition is

$$\phi(x, y, 0) = \bar{\phi} + \text{rand}, \qquad \psi(x, y, 0) = 0,$$

where rand is a random number between -0.1 and 0.1 at the grid points. The method $\mathrm{CS}_{\mathrm{BF}}(2)$ is used to examine the evolution from a random nonequilibrium state to a steady state. For saving computational time, we choose different time steps as the solution evolves from random noisy stage to relatively smooth stage. Although we do not try an adaptive time marching algorithm, we choose relatively fine time step $\Delta t = 2^{-12}$ for $0 < t \leq 20$ and coarse time step $\Delta t = 2^{-9}$ for $20 < t \leq 200$ based on the observation that smaller time step is needed with a random noisy initial condition in Section 4.5 compared to a smooth one in Section 4.2. Note that the method $\mathrm{CS}_{\mathrm{BF}}(2)$ is a multi-step method and a multi-step method may make the use of adaptive time step more difficult than a single-step method. In this paper, when a time step changes from the fine time step ($\Delta t = 2^{-12}$) to the coarse time step ($\Delta t = 2^{-9}$), we simply choose the solution before 8 fine time steps as the solution at $n-1$ time level. Figs. 15 and 17 show consistency error of the energy $\mathcal{F}(t)$ and our choice $\Delta t = 2^{-12}$ for early stage and $\Delta t = 2^{-9}$ for later stage seems to provide at least a single digit of accuracy.

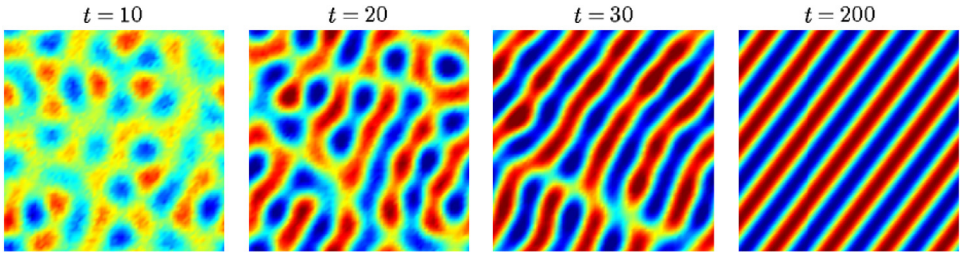

Fig. 14. Evolution of $\phi(x, y, t)$ with $\bar{\phi} = 0.02$, $\beta = 0.1$, $\epsilon = 0.2$, and $\Delta t = 2^{-12}$ for $0 < t \leq 20$ and $\Delta t = 2^{-9}$ for $20 < t \leq 200$. In each snapshots, the red, green, and blue regions indicate $\phi = 0.5318$, 0.0189, and -0.4940, respectively. (For interpretation of the references to color in this figure legend, the reader is referred to the web version of this article.)

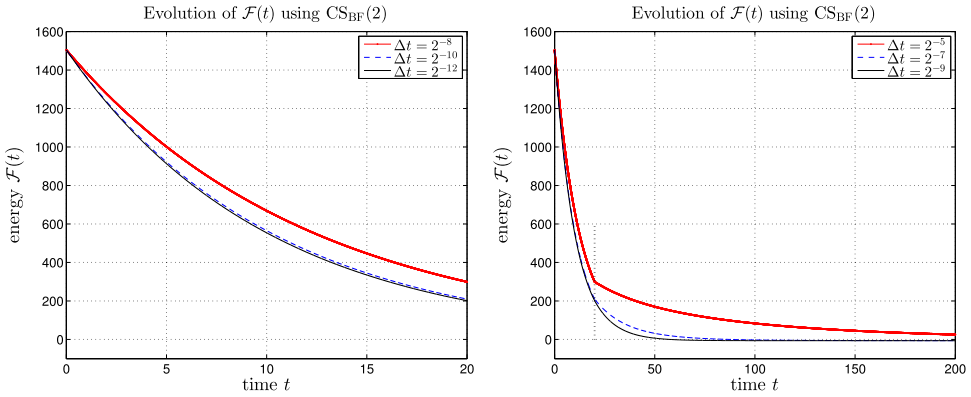

Fig. 15. Evolution of the energy $\mathcal{F}(t)$ for $\bar{\phi} = 0.02$ with different time steps. Numerical solution $\phi(x, y, t)$ for $20 < t \leq 200$ starts from a solution $\phi(x, y, t = 20)$ computed with finer time step $\Delta t/8$ for $0 < t \leq 20$.

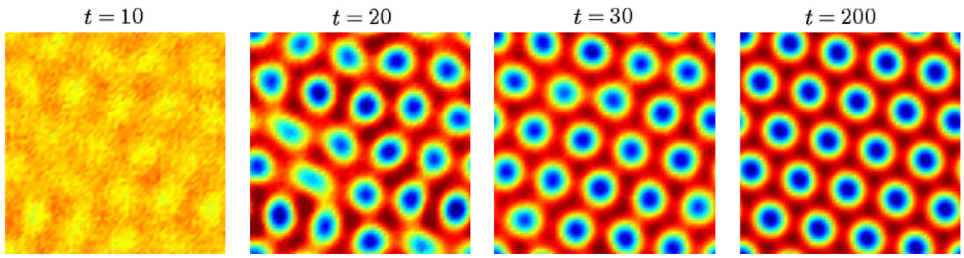

Fig. 16. Evolution of $\phi(x, y, t)$ with $\bar{\phi} = 0.2$, $\beta = 0.1$, $\epsilon = 0.2$, and $\Delta t = 2^{-12}$ for $0 < t \leq 20$ and $\Delta t = 2^{-9}$ for $20 < t \leq 200$. In each snapshots, the red, green, and blue regions indicate $\phi = 0.5547$, 0.0096, and -0.5355, respectively. (For interpretation of the references to color in this figure legend, the reader is referred to the web version of this article.)

Two simulations have been performed with $\bar{\phi} = 0.02$ and $\bar{\phi} = 0.2$ to verify that the method $\mathrm{CS}_{\mathrm{BF}}(2)$ does lead to the expected states in the phase diagram in [11]. For $\bar{\phi} = 0.02$, Figs. 14 and 15 show he evolution of $\phi(x, y, t)$ and $\mathcal{F}(t)$ with different time steps, respectively. Figs. 16 and 17 show those for $\bar{\phi} = 0.2$. Depending on the value of $\bar{\phi}$, we have different patterns, such as stripes (Fig. 14) and triangles (Fig. 16). Both results are consistent with the phase diagram in [11].

4.7. Crystal growth in 3D

We finally simulate the growth and interaction of two crystallites that originate from two nucleation sites on $\Omega = [0, 128] \times [0, 128] \times [0, 128]$ with $\beta = 1$, $M = 1$, $\epsilon = 0.25$, $\Delta x = \Delta y = \Delta z = 1$, and $\Delta t = 1$. An initial condition is generated as follows: we let a randomly perturbed constant state $\phi(x, y, z, 0) = 0.285 + \text{rand}$

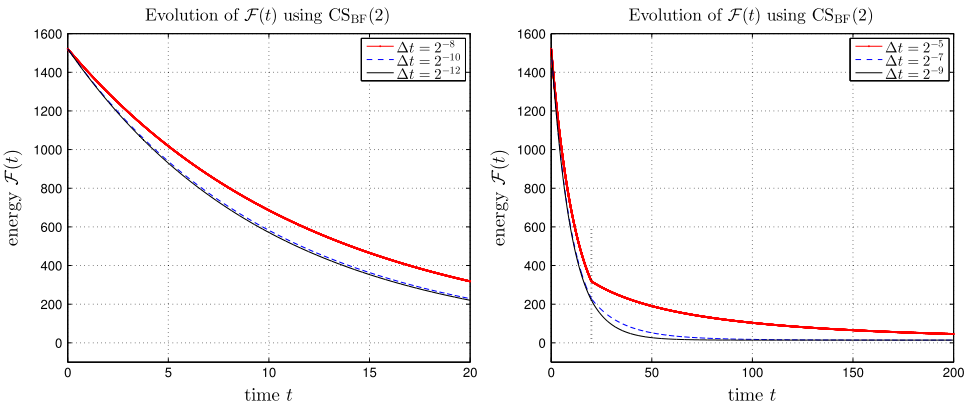

Fig. 17. Evolution of the energy $\mathcal{F}(t)$ for $\bar{\phi} = 0.2$ with different time steps. Numerical solution $\phi(x, y, t)$ for $20 < t \leq 200$ starts from a solution $\phi(x, y, t = 20)$ computed with finer time step $\Delta t/8$ for $0 < t \leq 20$.

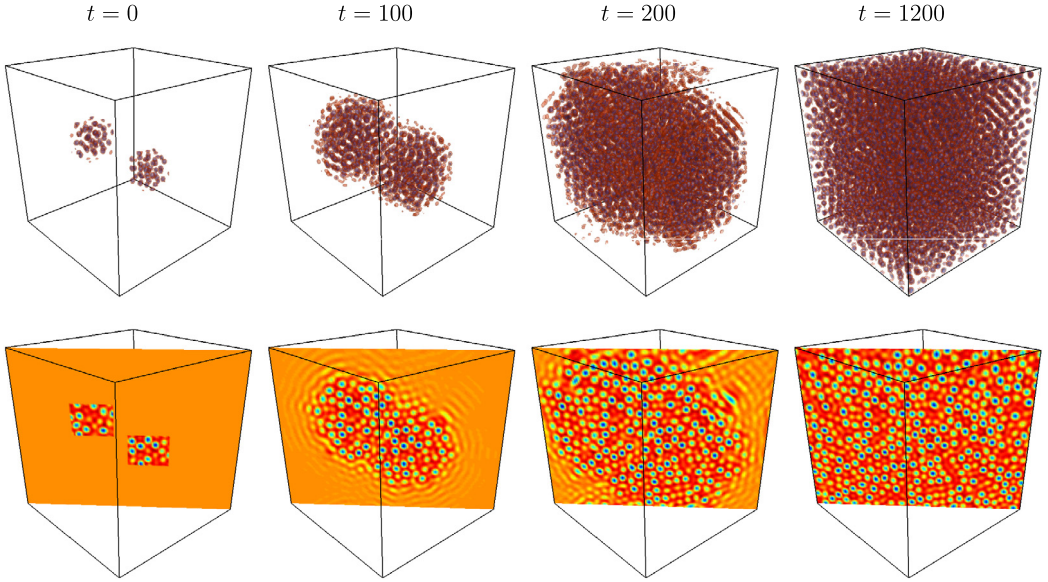

Fig. 18. Evolution of $\phi(x, y, z, t)$ with $\beta = 1$ and $\epsilon = 0.25$. The first and second rows show isosurfaces of ϕ and a slice of ϕ across the indicated plane, respectively. In each snapshots, the red, green, and blue regions indicate $\phi = 0.6813$, -0.0331, and -0.7475, respectively. (For interpretation of the references to color in this figure legend, the reader is referred to the web version of this article.)

with $\psi(x, y, z, 0) = 0$ evolve to a periodic lattice state, where rand is a random number between -0.1 and 0.1 at the grid points. We then extract two pieces of the final state with a hexahedral shape, and superpose them to a constant density field $\phi(x, y, z, 0) = 0.285$ with $\psi(x, y, z, 0) = 0$ (see the first column of Fig. 18). Figs. 18 and 19 show the evolution of $\phi(x, y, z, t)$ and $\mathcal{F}(t)$, respectively, using the method $\mathrm{CS}_{\mathrm{BF}}(2)$. We can see the interaction between growing crystallites and the energy dissipation.

5. Conclusions

The MPFC equation is a sixth-order nonlinear damped wave equation and cannot generally be solved analytically, thus, numerical methods are commonly used to study the dynamics of the MPFC equation. One criterion for developing a numerical method for the MPFC equation is whether the method inherits the energy dissipation property

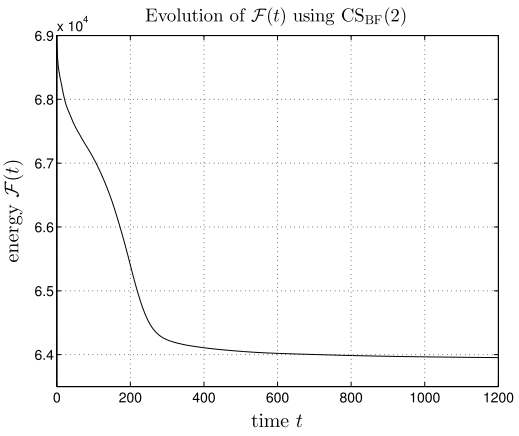

Fig. 19. Evolution of the energy $\mathcal{F}(t)$ with $\beta = 1$ and $\epsilon = 0.25$.

of the MPFC equation. To this, we presented temporally first- and second-order energy stable methods for the MPFC equation, which are based on the convex splitting of the energy for the PFC equation. The first- and second-order methods were shown analytically to be unconditionally stable with respect to the energy and pseudoenergy for the MPFC equation, respectively. We numerically compared with the existing other splitting methods $\mathrm{CS}_{\mathrm{DF}}$ to demonstrate the accuracy and energy stability of the proposed methods $\mathrm{CS}_{\mathrm{BF}}$ and observed that both methods $\mathrm{CS}_{\mathrm{DF}}$ and $\mathrm{CS}_{\mathrm{BF}}$ have the same order of convergence; however, the methods $\mathrm{CS}_{\mathrm{BF}}(1)$ and $\mathrm{CS}_{\mathrm{BF}}(2)$ are more accurate than the methods $\mathrm{CS}_{\mathrm{DF}}(1)$ and $\mathrm{CS}_{\mathrm{DF}}(2)$, respectively, from the perspective of error constant and numerical dissipation. We also observed that the time step effect on the energy evolution is more alleviated using the methods $\mathrm{CS}_{\mathrm{BF}}(1)$ and $\mathrm{CS}_{\mathrm{BF}}(2)$ than $\mathrm{CS}_{\mathrm{DF}}(1)$ and $\mathrm{CS}_{\mathrm{DF}}(2)$, respectively. From the results in this paper, we concluded that the proposed methods $\mathrm{CS}_{\mathrm{BF}}$ represent a good balance between accuracy and energy stability.

Acknowledgments

The authors thank the reviewers for the constructive and helpful comments on the revision of this article. The first author (H.G. Lee) was supported by the Research Grant of Kwangwoon University in 2017 and by Basic Science Research Program through the National Research Foundation of Korea (NRF) funded by the Ministry of Education (NRF-2016R1A6A3A11935668). The second (J. Shin) and corresponding (J.-Y. Lee) authors were supported by Basic Science Research Program through the National Research Foundation of Korea (NRF) funded by the Korea government MOE (2009-0093827) and MSIP (2015-003037).

References

[1] K.R. Elder, M. Katakowski, M. Haataja, M. Grant, Modeling elasticity in crystal growth, Phys. Rev. Lett. 88 (2002) 245701.
[2] K.R. Elder, M. Grant, Modeling elastic and plastic deformations in nonequilibrium processing using phase field crystals, Phys. Rev. E 70 (2004) 051605.
[3] J. Swift, P.C. Hohenberg, Hydrodynamic fluctuations at the convective instability, Phys. Rev. A 15 (1977) 319.
[4] H. Gomez, X. Nogueira, An unconditionally energy-stable method for the phase field crystal equation, Comput. Methods Appl. Mech. Engrg. 249–252 (2012) 52–61.
[5] N. Provatas, J.A. Dantzig, B. Athreya, P. Chan, P. Stefanovic, N. Goldenfeld, K.R. Elder, Using the phase-field crystal method in the multi-scale modeling of microstructure evolution, JOM 59 (2007) 83–90.
[6] P. Stefanovic, M. Haataja, N. Provatas, Phase-field crystals with elastic interactions, Phys. Rev. Lett. 96 (2006) 225504.
[7] P. Stefanovic, M. Haataja, N. Provatas, Phase field crystal study of deformation and plasticity in nanocrystalline materials, Phys. Rev. E 80 (2009) 046107.
[8] C. Wang, S.M. Wise, An energy stable and convergent finite-difference scheme for the modified phase field crystal equation, SIAM J. Numer. Anal. 49 (2011) 945–969.
[9] J. Shin, H.G. Lee, J.-Y. Lee, First and second order numerical methods based on a new convex splitting for phase-field crystal equation, J. Comput. Phys. 327 (2016) 519–542.
[10] M. Dehghan, V. Mohammadi, The numerical simulation of the phase field crystal (PFC) and modified phase field crystal (MPFC) models via global and local meshless methods, Comput. Methods Appl. Mech. Engrg. 298 (2016) 453–484.

[11] P.K. Galenko, H. Gomez, N.V. Kropotin, K.R. Elder, Unconditionally stable method and numerical solution of the hyperbolic phase-field crystal equation, Phys. Rev. E 88 (2013) 013310.
[12] S.M. Wise, C. Wang, J.S. Lowengrub, An energy-stable and convergent finite-difference scheme for the phase field crystal equation, SIAM J. Numer. Anal. 47 (2009) 2269–2288.
[13] Z. Hu, S.M. Wise, C. Wang, J.S. Lowengrub, Stable and efficient finite-difference nonlinear-multigrid schemes for the phase field crystal equation, J. Comput. Phys. 228 (2009) 5323–5339.
[14] A. Baskaran, Z. Guan, J. Lowengrub, Energy stable multigrid method for local and non-local hydrodynamic models for freezing, Comput. Methods Appl. Mech. Engrg. 299 (2016) 22–56.
[15] H.G. Lee, J. Kim, A simple and efficient finite difference method for the phase-field crystal equation on curved surfaces, Comput. Methods Appl. Mech. Engrg. 307 (2016) 32–43.
[16] D.J. Eyre, An unconditionally stable one-step scheme for gradient systems, unpublished article.
[17] A. Baskaran, Z. Hu, J.S. Lowengrub, C. Wang, S.M. Wise, P. Zhou, Energy stable and efficient finite-difference nonlinear multigrid schemes for the modified phase field crystal equation, J. Comput. Phys. 250 (2013) 270–292.
[18] M. Dehghan, V. Mohammadi, The numerical solution of Cahn–Hilliard (CH) equation in one, two and three-dimensions via globally radial basis functions (GRBFs) and RBFs-differential quadrature (RBFs-DQ) methods, Eng. Anal. Bound. Elem. 51 (2015) 74–100.
[19] F. Guillén-González, G. Tierra, On linear schemes for a Cahn–Hilliard diffuse interface model, J. Comput. Phys. 234 (2013) 140–171.
[20] J.W. Cahn, J.E. Hilliard, Free energy of a nonuniform system. I. Interfacial free energy, J. Chem. Phys. 28 (1958) 258–267.
[21] J.W. Cahn, On spinodal decomposition, Acta Metall. 9 (1961) 795–801.